Shock-Interaction-Induced Heat Transfer to the Orbiter Wing Lower Surface

David A. Throckmorton* and Lin C. Hartung†
NASA Langley Research Center, Hampton, Virginia

Flight-derived aerodynamic heat-transfer data for the Shuttle Orbiter wing lower surface, from STS-2, -3, and -5, are presented and compared with both ground-based experimental results and state-of-the-art computational flowfield results for a nominal angle of attack of 40 deg. The flight data clearly show the development of the interference heat-transfer region on the wing lower surface resulting from the downstream effects of the bow-shock/wing-shock interaction. The location of the interference heating region is well correlated with a region of minimum static enthalpy near the boundary-layer edge as predicted by a three-dimensional, inviscid flowfield computation. The magnitude of the interference heat transfer is no greater than the undisturbed laminar heat transfer occurring during the "peak aerodynamic heating" portion of re-entry.

Nomenclature

L	= scaled Orbiter characteristic length, = 32.77 m (107.5 ft) full scale
M	= freestream Mach number
q	= convective heat-transfer rate
q_{ref}	= heat-transfer rate to the stagnation point of a scaled 0.305 m (1 ft) radius sphere
R_L	= freestream Reynolds number based on orbiter characteristic length
$\bar{V}$	= viscous interaction parameter, $= M/\sqrt{R_L}$
x/c	= nondimensional longitudinal distance measured from wing leading edge
$Y/b/2$	= nondimensional spanwise distance measured from plane of symmetry
α	= angle of attack
γ	= "effective" ratio of specific heats

Introduction

THE initial flights (STS-1 through STS-5) of the Space Shuttle Orbiter Columbia, with its onboard instrumentation system, have provided a large body of flight heat-transfer data obtained over the entire entry flight regime. In conjunction with the extensive ground-derived data base for the Orbiter configuration, the existence of the flight data provides the aerothermodynamic researcher with the basic information required to assess the capability of ground-based facilities to simulate the flight heating environment about a lifting entry vehicle and to assess the utility of currently used techniques for ground-to-flight extrapolation of heat-transfer results. A number of researchers[1-8] have begun this process through analyses of various aspects of the entry aerothermal environment: such as leeside heat transfer,[2] windward-centerline heat transfer,[3-5] and surface catalysis effects on heat transfer.[6-8] (These cited references are representative of ongoing data analysis activities, but by no means comprise an exhaustive bibliography.) However, those detailed analyses of windward heat transfer appearing in the literature universally focus on the centerline results only. With the exception of Ref. 9, which does present some representative data (but only at a single flight condition), the literature contains no analyses of flight heat-transfer results for the wing lower surface.

The aerodynamic heating environment of the wing is produced by a portion of the Orbiter flowfield that is far different from that which influences heating to the plane of symmetry. On the outboard portion of the wing, the inviscid flow is processed by the wing shock only and not influenced by the vehicle bow shock. Inboard, the inviscid flow may be processed by the bow shock only. And, of course, a portion of the wing is influenced by fluid processed through the region of interaction between the vehicle bow and wing shocks. This paper presents flight heat-transfer results for the wing lower surface from missions STS-2, -3, and -5. Comparisons are made between flight and wind tunnel results for a wide range of flight conditions. The downstream effect on surface heat transfer of the bow-shock/wing-shock interaction is specifically highlighted.

Flight Data Processing

Data Source

During the orbital flight test missions, the Orbiter was equipped with an instrumentation system referred to as the development flight instrumentation (DFI). The DFI was made up of over 4500 sensors, associated data-handling electronics and recorder, that provided data to enable postflight certification of Orbiter subsystems design. Included among the DFI were measurements of aerodynamic surface temperature at over 45 locations on the Orbiter wing lower surface (Fig. 1). These measurements were obtained from thermocouples mounted within the thermal protection system (TPS), in thermal contact with the TPS surface coating.[10] DFI temperature data were recorded once each second throughout the time period of re-entry from Earth orbit. The measurement surface temperature-time histories provide for determination of vehicle surface heat-transfer rates. DFI tape recorder malfunctions on missions STS-1 and STS-4 resulted in the loss of all thermal data during that portion of re-entry when the vehicle was not in communications contact with the ground. No data were obtained on these missions at flight Mach numbers above approximately 12. Consequently, only data from missions STS-2, -3, and -5 are considered herein.

Data Reduction

A one-dimensional, transient conduction analysis[1] was used to determine the convective heating rate to each measurement location. The flight-measured surface temperature data provided a time-dependent boundary condition for the analysis,

Presented as Paper 84-0227 at the AIAA 22nd Aerospace Sciences Meeting, Reno, NV, Jan. 9-12, 1984; submitted Feb. 7, 1984; revision submitted Aug. 24, 1984. This paper is declared a work of the U.S. Government and therefore is in the public domain.

*Aero-Space Technologist, Aerothermodynamics Branch, Space Systems Division. Member AIAA.

†Cooperative Education Student, Rensselaer Polytechnic Institute, Troy, NY. Student Member AIAA.

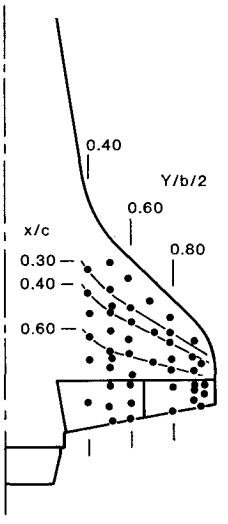

Fig. 1 Wing lower surface DFI temperature measurements.

which assumes an initially uniform temperature throughout the thermal protection materials. The analysis is a mathematically rigorous simulation of the heat conduction within the thermal protection system and reradiation from its surface, so as to provide a " benchmark" determination of the flight heat-transfer rates.

Flight Environment

Determination of the vehicle attitude and freestream flight environment data used herein was accomplished through reconstruction of the Orbiter's re-entry trajectory, reconstruction of the atmosphere on the day of re-entry, and correlation of these two data sets to provide an analytically consistent definition of the re-entry flight environment. The trajectory reconstruction process[11] utilizes ground-tracking data and onboard measurements of the Orbiter's inertial attitude, linear accelerations, and angular rates to determine the vehicle's inertial position, velocity, and attitude throughout the re-entry. The atmospheric reconstruction process[12] combines atmospheric modeling with direct measurement of atmospheric properties (pressure, temperature, density, and winds). The results of the trajectory and atmospheric reconstruction processes are melded together to provide an analytically and physically consistent definition of the freestream flight environment.

The reference heat-transfer rate q_{ref} used herein is that to the stagnation point of a 0.305 m (1 ft) radius sphere in radiation equilibrium at the flight condition. The real-gas heat-transfer rate computation was made by the method of Ref. 13 using the Fay and Riddell[14] expression for stagnation-point heat transfer.

Data Presentation and Analyses

The presentation of data in this paper will be limited to data obtained at a nominal Orbiter angle of attack of 40 deg. During each atmospheric re-entry flown to date, the Orbiter angle of attack was initially set at 40 deg and was maintained constant at that nominal value until the Orbiter passed through the maximum aerodynamic heating portion of the trajectory. (Trajectory control was accomplished by banking the vehicle about the velocity vector.) Thereafter, the angle of attack continually decreased as the transition to aircraft-like flight was made. While flying at the constant 40 deg angle of attack, the freestream Mach and Reynolds numbers varied over a wide range. During the angle-of-attack rampdown, however, only a single Mach/Reynolds number combination was experienced for any given angle of attack. Consequently, one can observe from the flight data the effects of Mach and Reynolds number variations on heat transfer only at a 40 deg angle of attack. At other angles of attack, one cannot observe such trends with the freestream parameters, as only one flight condition was traversed at each angle of attack. Additionally, the effects of Mach/Reynolds number and angle-of-attack variations on heat transfer are largely masked at lower angles of attack as the effects of boundary-layer transition dominate the surface heat transfer.[15]

Spanwise Heat-Transfer

The spanwise distributions of heat transfer to the wing lower surface for a range of freestream Reynolds number conditions from missions STS-2, -3, and -5 are shown in Fig. 2. Along the 30% chord (Fig. 2a), specifically on STS-2, it is observed that the nondimensional heat transfer inboard of the 50% semispan is relatively insensitive to changes in the freestream Reynolds number. At the 60% semispan location, however, the heating rate ratio is observed to be strongly dependent on the Reynolds number. This dependence probably results from a flow disturbance emanating from the vehicle bow-shock/wing-shock interaction region. Results from STS-3 and -5 (also Fig. 2a) are qualitatively similar to the STS-2 results. The data at the 60% semispan location are quantitatively different on STS-5 because the TPS surface at this location, on this mission only, had been coated with a highly catalytic material as part of an experiment[7] to investigate the catalytic efficiency of the baseline TPS surface coating relative to the recombination of dissociated oxygen atoms. (Comparison of the STS-5 results at this location with the STS-2 and -3 results indicates, as noted in Ref. 7, that chemical nonequilibrium significantly influences the level of heat transfer on the wing at these flight conditions.) Heat transfer at the 80% semispan location also reflects some Reynolds number dependence, but the level of sensitivity is not as significant as observed at the 60% semispan.

Along the 40% chordline (Fig. 2b), the heat transfer inboard of the 60% semispan is observed to be insensitive to Reynolds number. Heating which is strongly Reynolds-number dependent is evident at the 70% semispan. Apparently the path of the disturbance that causes the increased heat transfer moves outboard as it moves downstream. Outboard of the 70% semispan, some less significant heat-transfer sensitivity to Reynolds number is noted. Along this chordline, the results from all three flights are qualitatively similar.

Moving further downstream to the 60% chordline (Fig 2c), the nondimensional heat transfer is observed to be relatively insensitive to Reynolds number variation except, surprisingly, inboard at the 50% semispan and near the wing tip. Once again it is noted that the results from all three flights are qualitatively similar.

The correlation of heat transfer with Reynolds number at locations both without and within the disturbance region is more clearly illustrated in Fig. 3. At a location outside of the disturbance region (Fig. 3a, $Y/b/2 \approx 0.40$, $x/c \approx 0.40$, is typical), the nondimensional heat transfer is observed to be constant and independent of Reynolds number. At a location within the disturbance region (Fig. 3b, $Y/b/2 \approx 0.50$, $x/c \approx 0.60$), the nondimensional heat transfer is observed to be strongly dependent on Reynolds number. Comparisons of data from the three flights indicate that the heat-transfer rates increased from flight to flight at similar flight conditions. This has been observed by other investigators[6,7] and attributed to changes in the TPS surface emissivity and catalycity due to accumulated surface contamination.

Heat-Transfer Contour Plots

Contour plotting of the heat-transfer data provides a much clearer presentation of the heat-transfer distribution over the wing and also provides "mapping" of the downstream influence of the bow-shock/wing-shock interaction. Contour plots of the heat-transfer data at three STS-2 flight conditions are contained in Fig. 4 (where the flight conditions are the same as those at which the data were presented in Fig. 2). At the highest Mach number/lowest Reynolds number condition

	STS-2			STS-3			STS-5		
SYMBOL	α, deg	M	$R_L \times 10^{-6}$	α, deg	M	$R_L \times 10^{-6}$	α, deg	M	$R_L \times 10^{-6}$
○	39.8	26.1	0.56	40.1	22.7	0.56	40.1	26.4	0.55
□	40.4	24.6	0.92	40.4	20.8	0.92	40.4	23.2	0.92
◇	41.2	17.8	2.02	39.4	17.6	1.99	39.9	18.2	1.99
△	39.7	12.9	4.39	39.4	12.8	4.28	39.4	14.4	4.28

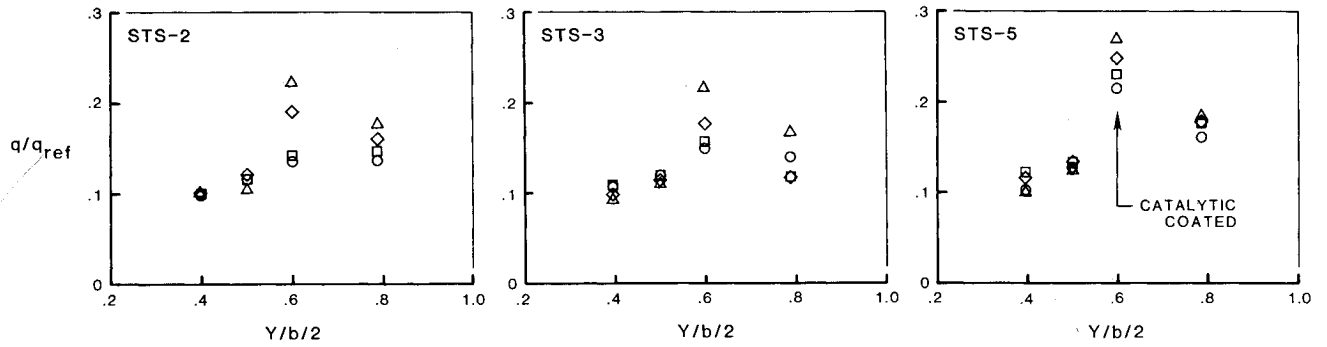

a) $x/c \approx 0.30$.

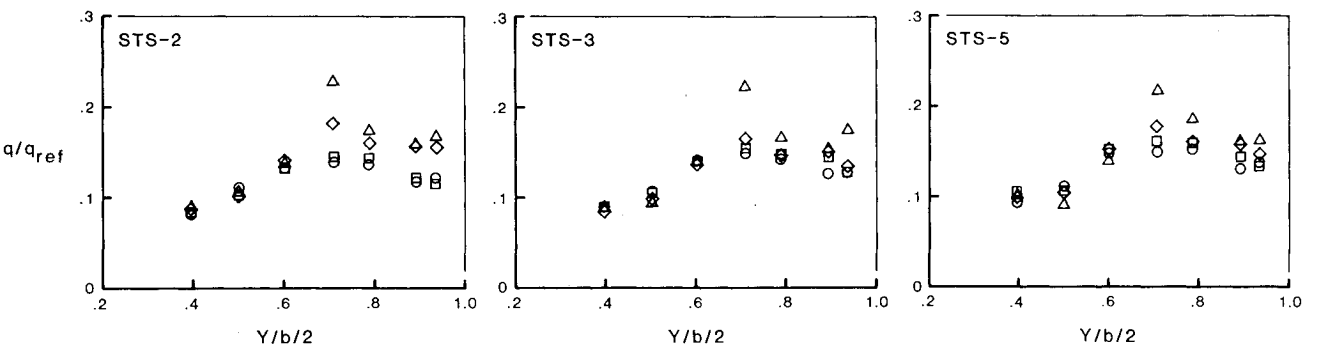

b) $x/c \approx 0.40$.

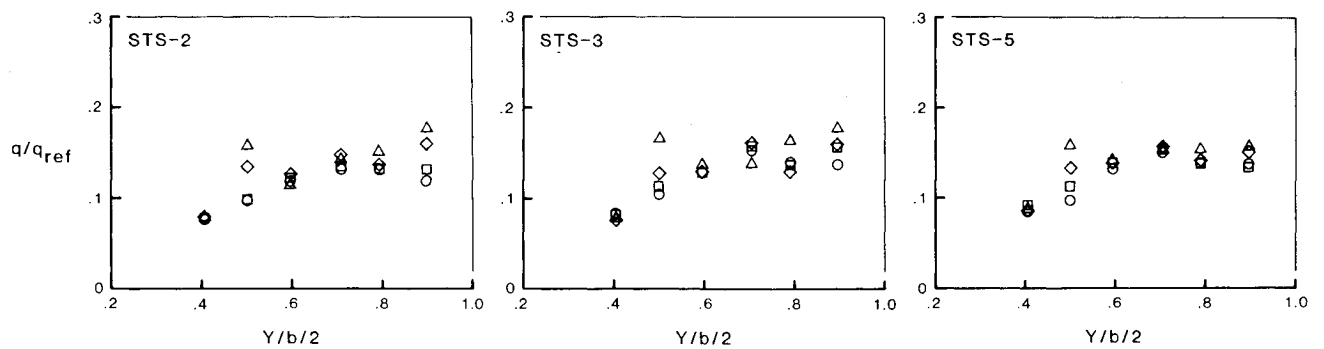

c) $x/c \approx 0.60$.

Fig. 2 Flight-derived spanwise heat-transfer distributions on the wing lower surface ($\alpha \approx 40$ deg).

(Fig. 4a), there is no evidence of shock interaction effects on surface heat transfer. As Reynolds number increases, however, the downstream influence of the shock/shock interaction on surface heat transfer begins to become apparent (Fig. 4b). At a still higher Reynolds number (Fig. 4c), the interference heating pattern resulting from the shock interaction becomes more distinctly defined and the nondimensional level of the heat transfer in the interference region becomes more severe.

On an Orbiter re-entry trajectory, an increasing Reynolds number relates to decreasing altitude and attendant increasing atmospheric density. At the flight condition of Fig. 4a, the Orbiter altitude was 75.9 km, an altitude at which the vehicle was flying in a very low density flow that could considered "transitional." (The value of the viscous interaction parameter $\bar{V}$ was approximately 0.025 at this flight condition. The flow is classically considered to be "transitional" for conditions of $\bar{V}$ greater than about 0.010.) At this flight condition, the flowfield within the vehicle shock structure is probably not characterized by distinct regions of inviscid flow and boundary-layer flow. Rather the flow is possibly better characterized as being a fully viscous shock-layer flow with no distinct surface boundary layer. Thus, it is not surprising that the shock-interaction disturbance should be quite diffuse and therefore not strong enough to manifest itself in a disturbance to the downstream surface heat transfer. At the flight condi-

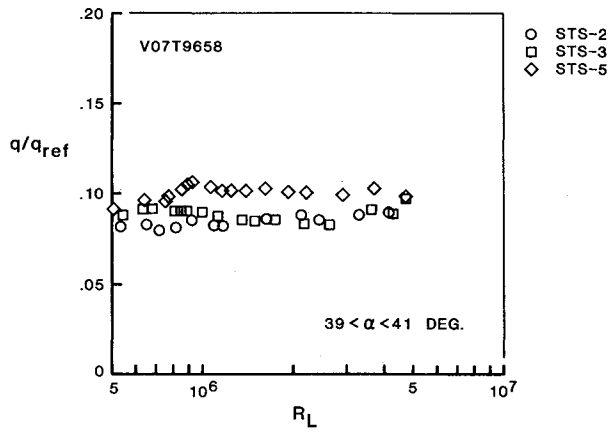

a) Outside of disturbance region ($Y/b/2 \approx 0.40$, $x/c \approx 0.40$).

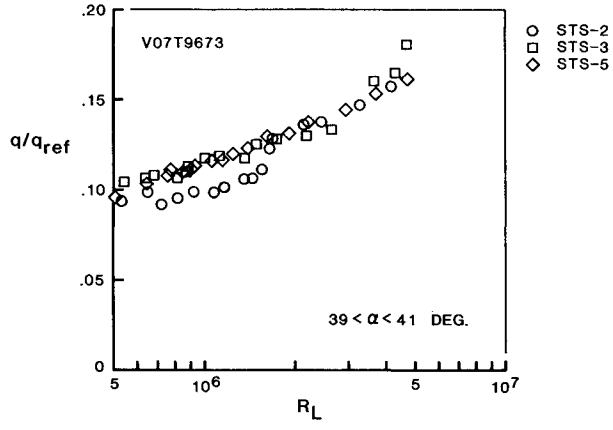

b) Within disturbance region ($Y/b/2 \approx 0.50$, $x/c \approx 0.60$).

Fig. 3 Reynolds number dependence of wing lower surface heat transfer.

tion of Fig. 4b, $\bar{V} \approx 0.012$; thus, the flow state is probably near continuum. At the flight condition of Fig. 4c, the viscous interaction parameter value ($\bar{V} \approx 0.006$) would indicate that the vehicle was flying in a continuum flow. Thus, the progressive strengthening of the downstream influence of the shock interaction on surface heat transfer is to be expected as the vehicle flowfield develops distinct inviscid and boundary layer regions between the shock envelope and the body.

Although, as has been shown, the nondimensional surface heat transfer to the wing is increased significantly by the downstream disturbance emanating from the shock-interaction region, it must be noted that this phenomenon occurs after the vehicle has passed the entry period of peak aerodynamic heating. Thus, the absolute magnitude of the interaction surface heat transfer is less than either the peak, undisturbed laminar heat transfer or, following boundary-layer transition, the turbulent heat transfer.

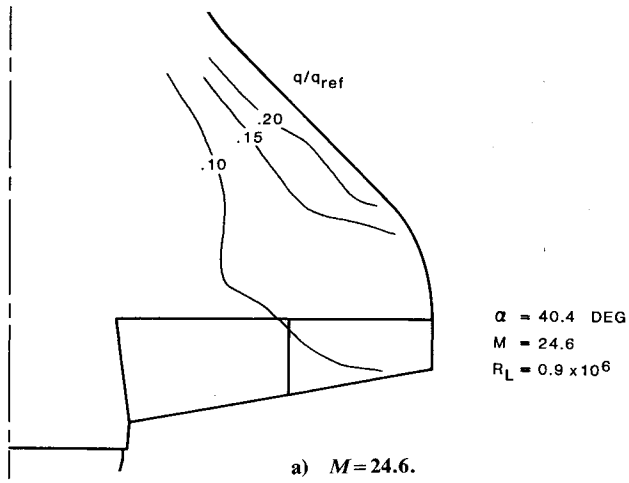

a) $M = 24.6$.

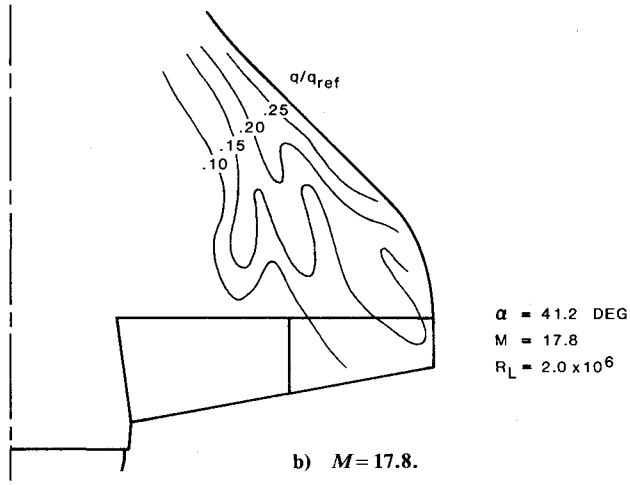

b) $M = 17.8$.

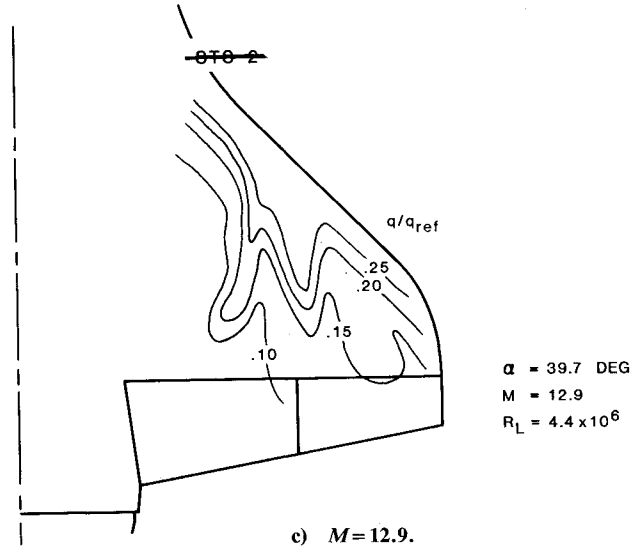

c) $M = 12.9$.

Fig. 4 STS-2 wing lower surface heat-transfer distributions.

Ground Test Results

Typical spanwise distributions of heat transfer to the wing derived from wind tunnel tests are contained in Fig. 5. These data were obtained at Mach 8 on a 0.0175 scale model instrumented with thermocouples. Along the 30 and 40% chordlines (Figs. 5a and 5b), there is no evidence of locally enhanced heating due to any downstream effect of the bow-shock/wing-shock interaction. At the 60% chordline (Fig. 5c), inboard of the 50% semispan, there is some increase in the heat transfer with increasing Reynolds number; however, inspection of the chordwise heating distributions (not shown herein) at these spanwise positions indicates that the heating increases are related to the boundary-layer transition and not to the shock-interaction disturbances. Apparently, in these wind-tunnel tests, either the shock interaction disturbance was not sufficiently strong to affect the surface heat transfer or the thermocouples were not positioned where the shock-interaction disturbance would be evident.

Another example of wind-tunnel-derived heating results is shown in Fig. 6. These data were obtained[17] on a 0.0175 scale "phase-change-paint" model also at Mach 8. It can be seen that with the spatial detail of information obtained using the phase-change testing technique, the surface heat-transfer

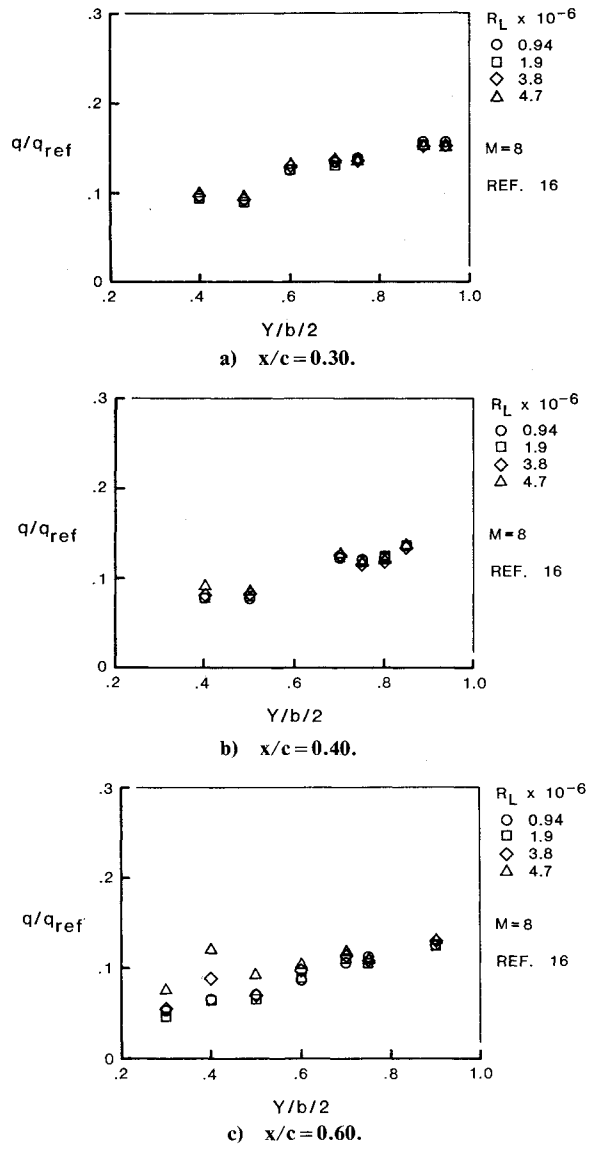

Fig. 5 Wind-tunnel-derived spanwise heat-transfer distributions on the wing lower surface ($\alpha = 40$ deg).

response to the shock-interaction disturbance is readily apparent. The test conditions at which these data were obtained are roughly equivalent (in freestream Reynolds number) to those of a flight condition between those of Figs. 4b and 4c.

A comparison of the wind-tunnel (Fig. 5) and flight (Fig. 2) results indicates not only differences in the observed interference heat transfer, but also reveals some differences in the "undisturbed" spanwise heating distributions. The differences are especially evident outboard of the 50% semispan at both the 40 and 60 % chordlines. The heat-transfer results derived from the wind tunnel tests (expressed in the nondimensional form q/q_{ref}) are, in general, significantly lower than the flight results along these chordlines. Not unexpectedly, this suggests that the direct application of wind-tunnel-derived q/q_{ref} values at flight conditions is not appropriate for the wing lower surface data. Rather, a method of scaling the ground-derived data to the flight environment is required. The heating methodology applied to orbiter TPS design utilized wing tunnel results to "calibrate" simple two-dimensional flowfield solutions.[18] These "calibrated" two-dimensional flowfield methods were then applied at the flight conditions to predict the flight heating environment. The limited results presented in Ref. 9 at these chordwise locations suggest that this scaling approach was adequate for the Orbiter TPS design.

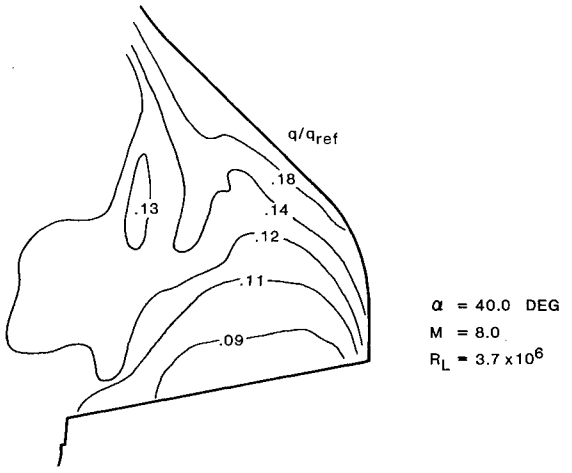

Fig. 6 Wing lower surface heat-transfer distribution derived from wind tunnel data.

Computational Predictions

Weilmuenster and Hamilton[19] have developed a numerical procedure for computing the three-dimensional, inviscid flowfield about Shuttle-like configurations at high angle of attack. The computer code, referred to as HALIS (high alpha inviscid solution), has been shown[20] to produce accurate predictions of flight surface pressures on the Orbiter wing lower surface and detailed flowfield information in the wing-shock/bow-shock interaction region. The HALIS procedure has not yet been linked to a boundary-layer solution to provide computation of surface heat transfer. However, in a complex flowfield like that existing on the Orbiter wing, one might expect that the values of inviscid flow parameters at the boundary-layer edge would provide a qualitative indication of the complexity of the expected surface heat-transfer distribution. With this assumption in mind, HALIS results were used to produce contour plots of static enthalpy at approximately the boundary-layer edge over the entire wing lower surface for several STS-3 entry flight conditions. The HALIS computations were performed using an ideal-gas formulation with assumed "effective gammas" to account for real-gas effects.

Typical comparisons of the HALIS flowfield results with STS-3 flight-derived heat-transfer results are contained in Fig. 7 for two flight conditions. At a moderate Mach/Reynolds number flight condition (Fig. 7a), the HALIS results indicate the presence of a distinct "minimum" in the spanwise distributions of boundary-layer edge static enthalpy downstream of the shock/shock interaction region. The developing influence of the shock/shock interaction at this flight condition is also evidenced in the "maximum" streak in the flight-derived downstream surface heat transfer. The spatial location of the "minimum" in the computed boundary-layer edge enthalpy correlates well with the location of the "maximum" in the flight-observed surface heat transfer. At a lower Mach/higher Reynolds number condition (Fig. 7b), the "minimum" in the HALIS enthalpy results is observed to have moved slightly outboard when compared to the previous case, primarily as a result of the change in effective gamma. The flight-derived interference heat-transfer region is observed to be quite distinct at this flight condition. Again there is excellent correlation between the locations of the HALIS-computed enthalpy "minimum" and the flight-observed heat-transfer "maximum."

A local minimum in boundary-layer-edge static enthalpy relates to a local increase in boundary-layer-edge velocity. Apparently, the shock interaction generates a downstream "jet" of fluid moving at an increased velocity. In flight, this could be expected to result in local thinning of the boundary layer and thus increased heat transfer to the the underlying surface.

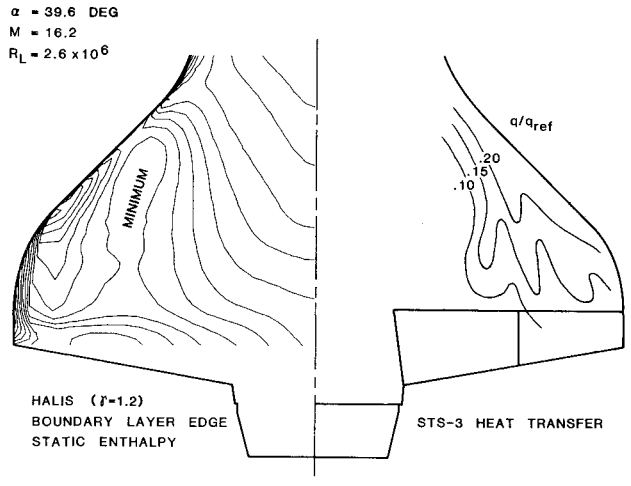

a) $M = 16.2$.

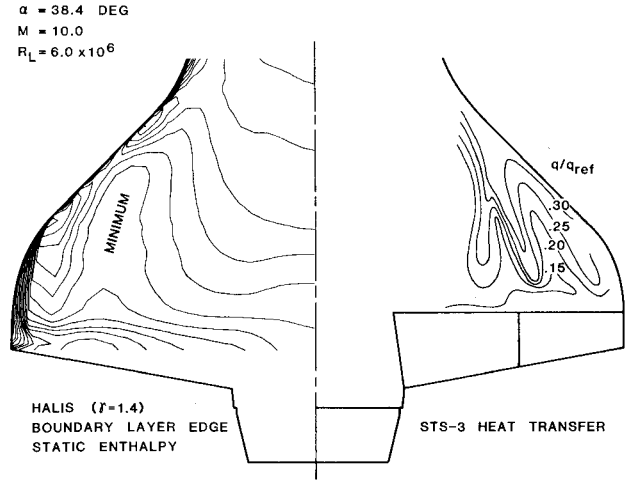

b) $M = 10.0$.

Fig. 7 Comparisons of STS-3 flight-derived heat-transfer distributions and computed boundary-layer-edge enthalpy distributions for the wing lower surface.

No comparisons are made between the HALIS-computed flowfield and the flight heat-tranfer results at high Mach/altitude conditions (such as that of Fig. 4a). The HALIS solution assumes a continuum, inviscid flow in the shock layer with a thin, distinct boundary layer. As has been previously discussed, along an Orbiter entry trajectory at high altitude/Mach numbers, the flow about the Orbiter is not necessarily a continuum and the inviscid and boundary-layer regions of the flow are probably not distinct. The flowfield is probably better described as a fully viscous shock layer. Therefore, one would not expect good correlation between HALIS and flight results at those flight conditions.

Conclusions

Flight-derived aerodynamic heat-transfer data for the Orbiter wing lower surface, from STS-2, -3, and -5, have been presented and compared with both ground-based experimental results and state-of-the-art computational flowfield results for a nominal angle of attack of 40 deg. The flight heat-transfer data show clearly the progressive development, as its re-entry trajectory carries the Orbiter deeper into the atmosphere, of the interference heat-transfer region on the wing lower surface resulting from the downstream effects of the bow-shock/wing-shock interaction. At 40 deg angle of attack, the interference heating pattern on the wing appears to be much more distinct in flight than in the wind tunnel. Quantitatively, at locations on the wing surface not affected by the shock interaction disturbance, the nondimensional heat transfer (q/q_{ref}) in flight is significantly greater than that measured in ground-based facilities. This suggests that direct application of wind-tunnel-derived q/q_{ref} values at flight conditions is not appropriate for wing lower surface data. Rather a method of scaling the ground-derived data to the flight environment is required. Comparison of flight heat-transfer contours on the wing surface with boundary-layer-edge enthalpy contours produced by a state-of-the-art inviscid computational procedure reveals an excellent correlation between locations of measured "maximum" heat transfer and predicted "minimum" edge enthalpy. The magnitude of the shock-interaction-induced interference heat transfer is no greater than the undisturbed laminar heat transfer that occurs during the "peak aerodynamic heating" portion of entry.

Acknowledgment

The authors express their sincere appreciation to K. J. Weilmuenster for providing the HALIS inviscid flowfield solution results presented herein.

References

[1]Throckmorton, D. A., "Benchmark Determination of Shuttle Orbiter Entry Aerodynamic Heat-Transfer Data," *Journal of Spacecraft and Rockets,* Vol. 20, May-June 1983, pp. 219-224.

[2]Throckmorton, D. A. and Zoby, E. V., "Orbiter Entry Leeside Heat-Transfer Data Analysis," *Journal of Spacecraft and Rockets,* Vol. 20, Nov.-Dec. 1983, pp. 524-530.

[3]Zoby, E. V., "Comparisons of STS-1 Experimental and Predicted Heating Rates," *Journal of Spacecraft and Rockets,* Vol. 20, May-June 1983, pp. 214-218.

[4]Zoby, E. V., "Analysis of STS-2 Experimental Heating Rates and Transition Data," *Journal of Spacecraft and Rockets,* Vol. 20, May-June 1983, pp. 232-237.

[5]Hamilton, H. H. II, "Approximate Method of Predicting Heating on the Windward Side of Space Shuttle Orbiter and Comparisons with Flight Data," *AIAA Progress in Astronautics and Aeronautics: Entry Vehicle Heating and Thermal Protection Systems: Space Shuttle, Solar Starprobe., Jupiter Galileo Star Probe,* Vol. 85, edited by P. E. Bauer and H.E. Collicott, AIAA, New York, 1983, pp. 21-53.

[6]Scott, C. D., "A Review of Nonequilibrium Effects and Surface Catalysis on Shuttle Heating," NASA CP-2283, 1983, pp. 865-889.

[7]Stewart, D. A., Rakich, J. V., and Lanfranco, M. J., "Catalytic Surface Effects on Space Shuttle Thermal Protection System During Earth Entry of Flights STS-2 through STS-5," NASA CP-2283, 1983, pp. 827-845.

[8]Harthun, M. H., Blumer, C. B., and Miller, B. A., "Orbiter Windward Surface Entry Heating: Post-Orbital Flight Test Program Update," NASA CP-2283, 1983, pp. 781-804.

[9]Williams, S. D. and Curry, D. M., "An Assessment of the Space Shuttle Orbiter Thermal Environment Using Flight Data," AIAA Paper 83-1488, June 1983.

[10]Stoddard, L. W. and Draper, H. L., "Development and Testing of Development Flight Instrumentation for the Space Shuttle Thermal Protection System," *Proceedings of the 24th International Symposium,* Instrument Society of America, Pittsburgh, Pa., 1978.

[11]Compton, H. R., Findlay, J. T., Kelly, G. M., and Heck, M. L., "Shuttle (STS-1) Entry Trajectory Reconstruction," AIAA Paper 81-2459, Nov. 1981.

[12]Price, J. M., "Atmospheric Definition for Shuttle Aerothermodynamic Investigations," *Journal of Spacecraft and Rockets,* Vol. 20, March-April 1983, pp. 133-140.

[13]Hamilton, H. H. II, "Approximate Method of Calculating Heating Rates at General Three-dimensional Stagnation Points During Atmospheric Entry," NASA TM 84580, Nov. 1982.

[14]Fay, J. A. and Riddell, F. R., "Theory of Stagnation Point Heat Transfer in Dissociated Air," *Journal of the Aeronautical Sciences,* Vol. 25, Feb. 1958, pp. 73-85, 121.

[15]Hartung, L. C. and Throckmorton, D. A., "Computer Graphic Visualization of Orbiter Lower Surface Boundary-Layer Transition," AIAA Paper 84-0228, Jan. 1984.

[16]Herrera, B. J., "An Investigation of Entry Heating on the 0.0175 Scale Space Shuttle Orbiter (Model 60-0) in the AEDC VKF Tunnel B," NASA CR-160, 490, May 1980 (DMS-DR-2241).

[17]Dye, W. H., "Heat Transfer Phase Change Paint Tests of 0.0175-Scale Models (Nos. 21-0 and 46-0) of the Rockwell International Space Shuttle Orbiter in the AEDC Tunnel B Hypersonic Wind Tunnel (Test OH254A)," NASA CR-141546, July 1975 (DMS-DR-2252).

[18]Reid, R. C., "Orbiter Entry Aerothermodynamics," NASA CP-2342, 1985, pp. 1051-1061.

[19]Weilmuenster, K. J. and Hamilton, H. H. II, "Calculations of Inviscid Flow Over Shuttle-Like Vehicles at High Angles of Attack and Comparisons With Experimental Data," NASA TP 2103, 1983.

[20]Weilmuenster, K. J., "High Angle of Attack Inviscid Flow Calculations Over a Shuttle-Like Vehicle With Comparisons to Flight Data," AIAA Paper 83-1798, July 1983.